The Impact of Tissue Type and Density on Dose Point Kernels for Patient-Specific Voxel-Wise Dosimetry: A Monte Carlo Investigation

Authors: Tiwari, Ashok, Gravesa, Stephen A., and Sunderland, John

Source: Radiation Research, 193(6) : 531-542

Published By: Radiation Research Society

URL: https://doi.org/10.1667/RR15563.1

RADIATION RESEARCH **193**, 531–542 (2020)
0033-7587/20 $15.00

DOI: 10.1667/RR15563.1

The Impact of Tissue Type and Density on Dose Point Kernels for Patient-Specific Voxel-Wise Dosimetry: A Monte Carlo Investigation

Ashok Tiwari,[a,b] Stephen A. Graves[a] and John Sunderland[a,b,1]

[a] *Department of Radiology, University of Iowa Hospitals and Clinics, Iowa City, Iowa 52242; and* [b] *Department of Physics, University of Iowa, Iowa City, Iowa 52242*

Tiwari, A., Graves, S. A. and Sunderland, J. The Impact of Tissue Type and Density on Dose Point Kernels for Patient-Specific Voxel-Wise Dosimetry: A Monte Carlo Investigation. *Radiat. Res.* 193, 531–542 (2020).

We report the generation of dose point kernels for clinically-relevant radionuclide beta decays and monoenergetic electrons in various tissues to understand the impact of tissue type on dose point kernels. Currently available voxel-wise dosimetry approaches using dose point kernels ignore tissue composition and density heterogeneities. Therefore, the study on the impact of tissue type on dose point kernels is warranted. Simulations were performed using the GATE Monte Carlo toolkit, which encapsulates GEANT4 libraries. Dose point kernels were simulated in phantoms of water, compact bone, lung, adipose tissue, blood and red marrow for radionuclides ^{90}Y, ^{188}Re, ^{32}P, ^{89}Sr, ^{186}Re, ^{153}Sm and ^{177}Lu and monoenergetic electrons (0.015–10 MeV). All simulations were performed by assuming an isotropic point source of electrons at the center of a homogeneous spherical phantom. Tissue-specific differences between kernels were investigated by normalizing kernels for effective pathlength. Transport of 20 million particles was found to provide sufficient statistical precision in all simulated kernels. The simulated dose point kernels demonstrate excellent agreement with other Monte Carlo packages. Deviation from kernels reported in the literature did not exceed a 10% global difference, which is consistent with the variability among published results. There are no significant differences between the dose point kernel in water and kernels in other tissues that have been scaled to account for density; however, tissue density predictably demonstrated itself to be a significant variable in dose point kernel distribution.

INTRODUCTION

Radioisotopes and their associated decay products play a central role in both imaging and therapeutic nuclear medicine applications. Radionuclides such as ^{90}Y, ^{32}P, ^{131}I, ^{111}In and ^{89}Sr have been used for several decades in both radiotherapy and single photon imaging applications, whereas ^{18}F, ^{68}Ga and ^{89}Zr are widely used in the PET imaging. In addition, ^{177}Lu and ^{223}Ra have recently attracted considerable attention and demonstrated great promise in targeted radionuclide therapy applications. Regardless of whether the radionuclides are tagged to imaging or therapy radiopharmaceuticals, irradiated molecules/atoms within cells absorb energy from the charged particles emitted from radionuclide decay and also from the photons when interacting with secondary charged particles. This energy deposition can promote direct macromolecular damage as well as generate reactive oxygen and/or nitrogen species (*1*).

Starting with a known distribution of radioactive decays in the body, the absorbed dose to tissues can be estimated using one of several techniques. The most rigorous dosimetric methods employ image-based radionuclide distributions combined with full Monte Carlo calculations, but this typically requires many hours to perform. The Medical Internal Radiation Dosimetry (MIRD) approach is perhaps the simplest and most widely used to calculate organ-specific internal radiation dose. The traditional MIRD formalism is an organ-based dosimetry technique, which uses pre-tabulated organ-based S values. The S value is the radionuclide-specific quantity representing the mean absorbed dose rate to a target organ per unit activity in a source organ (*2*). The limitations to this approach are severalfold. Activities in organs are assumed to be uniformly distributed. Also, the MIRD ''standard man'' assumes standard organ shapes and sizes with rigid geometric relationships between organs, and S values are not tabulated for distributions other than simple, whole organs. Although whole-organ dosimetry is colloquially what is meant by ''the MIRD method,'' it is worth noting that the absorbed fraction methodology can also be applied to organ sub-units, cells or at the voxel level (*2, 3*). The latest MIRD/ICRP voxel-based anthropomorphic phantoms

Editor's note. The online version of this article (DOI: https://doi.org/10.1667/RR15563.1) contains supplementary information that is available to all authorized users.

[1] Address for correspondence: PET Center, Department of Radiology, University of Iowa Hospitals and Clinics, Iowa City, IA 52242; email: john-sunderland@uiowa.edu.

are also available, however, tissue composition heterogeneity is not considered, and patient-specific organ geometries are not yet feasible (*4–6*).

Intra-organ dosimetry with nonuniform activity distributions has been addressed by development of voxel-based dosimetry, including the voxel S value (VSV) and the dose point kernel (DPK) methods. These methods rely on convolving isotope-specific kernels with the cumulative activity distribution of interest, such that a dose map is obtained. Dose kernels used for this process often follow the nomenclature ''VSV'' for kernels that are in voxelized coordinate space, and ''DPK'' for kernels that are tabulated as a function of radius from a point source, although this convention is not universally followed. Converting a DPK to a VSV map involves resampling the DPK into Cartesian coordinates and convolving with the uniform activity of a source voxel.

Empirical measurement of beta dose point kernels is challenging due to the limited range of electrons in matter and spatial limitations of conventional dosimeters. As such, many authors have calculated kernels analytically (*7*) or simulated them using Monte Carlo (MC) methods (*8–16*). Monte Carlo codes that have been used for this purpose include ETRAN, SMOOPY, EGSnrc, FLUKA, PENELOPE, MCNPX, Geant4DNA and GATE. All of these Monte Carlo codes attempt to approximate a solution to the Boltzmann transport equation by employing different treatments of stochastic transport processes.

The simulation of interactions between electrons and their secondary particles with matter is one of the main tasks of Monte Carlo simulations. The resulting energy deposition is relevant to a wide variety of applications. GATE, the Geant4 Application for Tomographic Emission, is an open-source package Monte Carlo simulation toolkit, which incorporates the Geant4 cross-section and stopping power data libraries (*17*). The GATE software has been extensively used in imaging applications since its release in May 2004 (*18*). Visvikis *et al*. (*19*) were the first to study the potential of GATE in dosimetric applications; similar dosimetric uses of GATE have been the subject of additional literature (*11, 20–24*). For the current study, we exclusively used the GATE Monte Carlo simulation toolkit (GATE version 8.1) to simulate the dose distribution of monoenergetic electrons and the beta spectra of several medically relevant radionuclides in several tissue types.

The simulation of beta-emitting radionuclides and monoenergetic electrons in different materials is essential to understanding the impact of tissue type on the spatial distribution of energy deposition. In this work, we simulate electrons and betas in different tissues: water, compact bone (hereafter bone), blood, red marrow, adipose and lung. Monoenergetic electrons dose point kernels were simulated for energies (0.015–10 MeV). Variability of scaled kernels may inform of the utility of multi-kernel dosimetry methods, so comparison of kernels generated in different tissues was a priority within this work. In addition to monoenergetic electrons, dose point kernels were simulated for common therapeutic radionuclides: ^{90}Y, ^{188}Re, ^{32}P, ^{89}Sr, ^{186}Re, ^{153}Sm and ^{177}Lu. The beta emitters ^{90}Y, ^{188}Re, ^{186}Re and ^{177}Lu are isotopes used in targeted radiotherapy, whereas the isotopes ^{153}Sm, ^{89}Sr and ^{32}P are useful for the treatment of metastatic bone pain (*25*). Finally, a comparison of the dose point kernels in water and bone against other Monte Carlo codes was performed. The novel dataset of all GATE version 8.1-generated dose point kernels in media as mentioned above is included in the Supplementary Tables (https://doi.org/10.1667/RR15563.1.S1).

MATERIALS AND METHODS

Monte Carlo Simulation Using GATE

DPKs were simulated in a spherical phantom assuming a homogeneous spherical system with a point source at its center, emitting isotropically. Dose deposition was tabulated in spherical concentric shells placed around the source at fixed radial distances. The thickness of the concentric shells for each Monte Carlo simulation was made to be equal to the voxel size of the three-dimensional (3D) dose matrix (defined as the electron step size in the simulation). The dose scoring voxel volume has been defined as the dosel (*17*). In all simulations, the radius of the phantom was greater than the range of electrons in the homogeneous media.

Electrons, in passing through the matter, undergo physical interactions and lose energy primarily by ionization, although other processes (multiple scattering, bremsstrahlung, Cerenkov radiation, backscattering and Moller scattering losses) contribute as well. In this simulation using GATE, the electromagnetic (EM) constructor, ''emstandard_opt3,'' was implemented for the physics list. This EM constructor is useful for applications that require higher accuracy of electrons, hadrons and ion tracking (*26*).

The following parameters in GATE were used for all simulations: EMin = 0.1 keV, EMax = 10 GeV, DEDXBinning = 220 and LambdaBinning = 220. These parameters specify the kinetic energy range for all physical processes, the number of bins for the mean energy loss (default = 84) and the number of bins for the mean free path table (default = 84). Variance reduction techniques were not used in any of the simulations performed in this work.

In GATE, doseActor was used to calculate the energy deposition. The deposited energy, EDep, was scored at the voxel level, and associated uncertainties were calculated in each dosel with the doseActor UncertaintyEDep. The output of the simulation, i.e., 3D energy deposition matrices and its statistical uncertainties, were stored in the MetaImage format, i.e., mhd, as recommended by GATE (*17*). A MATLAB® in-house code was developed, which converts the cartesian coordinates to the polar coordinates, to obtain the relevant dosimetric quantities from the results. In this simulation work, deposited energies were scored into bins of size equal to the thickness of the concentric shells. To ensure at least one physical interaction in each bin, the bin width was set equal to the electronStepLimiter parameter, referred to as the Step-Max. The effective atomic number (Z_{eff}) and densities of simulated tissues are tabulated in Table 1. The atomic composition and densities of these materials were obtained from ICRU Report No. 46 (*27*).

Electron Step Size

During simulation, electron trajectories were divided into sub-steps, all of equal length, regardless of electron energy. The fixed step size scheme used herein also permits efficient implementation of the Goudsmit-Saunderson theory. The step length is usually chosen so that the energy loss along a step is constant. The MCNP (*28*) and

TABLE 1
The Densities and Effective Atomic Number of Tissues Used in Simulations

Materials	ρ (g/cm^2)	Z_{eff}
Bone	1.85	11.87
Blood	1.06	7.78
Lung	0.26	7.74
Water	1.00	7.42
Red marrow	1.03	7.21
Adipose	0.92	6.47

ETRAN code (*15*) have a default value of 8.3% average energy loss per step. However, in Geant4, the recommended value of fractional energy loss per step is 10% set by the parameter referred to as dRoverRange during a step for particle (*26, 29*).

Electron step size is a user-controlled parameter in simulation; the electronStepLimiter parameter was used to set the electron step. It was fixed by the corresponding percentage energy loss of the electrons in different media. To get more accurate results very small steps are optimal; however, simulation becomes computationally intensive as the step size decreases. The step size is calculated using the stopping power and energy of the electron. The fractional energy loss for each step is $\Delta E/E = \text{constant}$, where $\Delta E = E_n - E_{n-1}$ is given by:

$$\Delta E = -\int_{S_{n-1}}^{S_n} \frac{dE}{dS} dS, \tag{1}$$

where dE/dS is the total stopping power for the energy and material media of interest. The stopping power values were taken from the ESTAR database (*30*) to calculate the step length parameter. Electron step sizes were equal to the voxel sizes in all simulations performed herein.

Energy Thresholds

An energy threshold was set, below which the particle transport assumed local energy deposition, using the range cut parameter. This energy threshold is necessary to avoid the infrared divergences that appear in electromagnetic processes (*17*). In this work, where electron energy is greater than 1 MeV, energy thresholds of ~10 keV were set, for 100 keV to 1 MeV energy range, energy thresholds of ~5 keV were set and for 15–100 keV, the energy thresholds used were ~2 keV. For instance, the associated range thresholds at the energy threshold of 5 keV were: 3.1 μm in bone, 5.2 μm in blood, 5.3 μm in red marrow, 5.4 μm in water, 5.76 μm in adipose and 21 μm in lung.

Monoenergetic Electron Dose Point Kernels

The dose point kernels (DPKs) can be defined as energy deposition kernels from point isotropic sources. DPKs can also be described as the dose deposition profile, as a function of radial distance. For monoenergetic electrons, the scaled absorbed dose can be written as (*7, 31*):

$$J\frac{r}{R_{CSDA}} = 4\pi r^2 D(r)\frac{R_{CSDA}}{E_0}, \tag{2}$$

where r is the radial distance from the center of the sphere, $D(r)$ is the absorbed dose per source particle a distance r and R_{CSDA} is the range of electrons in the continuous slowing down approximation (CSDA) with source energy E_0. The nominal *CSDA* range (R_{CSDA}) tabulated in Table 2 for all energies was obtained from the NIST ESTAR database (accessed May 2019) (*30*). The values of R_{CSDA} tabulated in Table 2 are the ranges of electrons scaled with corresponding density of the material media in g/cm^2, and demonstrate a differential range of approximately 10%.

Use of the scaled kernel formalism given by Eq. (2) facilitates inter-kernel comparison by: 1. Normalizing the domain to R_{CSDA}; 2. Normalizing the range to the total electron energy; and 3. Removing the inverse-square dependence of energy deposition about an isotropic point source. The dimensionless quantity (J), defined by Eq. (2), represents the fraction of dose deposited in a spherical shell of scaled radius r/R_{CSDA} to $r/R_{CSDA} + d(r/R_{CSDA})$.

Twenty million primaries were simulated for each monoenergetic electron simulations. The dose point kernels for monoenergetic electrons with energies 15 keV, 50 keV, 100 keV, 500 keV, 1 MeV, 2 MeV, 4 MeV and 10 MeV were simulated in media of water, bone, blood, red marrow, adipose and lung; our work was compared with published literature (*8, 9, 11, 31, 32*).

The voxel sizes for each simulation were calculated using Eq (1) and were also used with preliminary simulations to check whether the calculated values are in good agreement with the results of other Monte Carlo codes. All voxel sizes for each simulation are provided in Tables 3 and 4. Moreover, for the voxel sizes for 50 keV, 500 keV and 2 MeV monoenergetic electrons in water were made to match with those used by Papadimitroulas *et al.* (*11*) for comparison with their work.

Beta Emitter Radionuclides Dose Point Kernels

All simulation parameters were maintained when moving to beta spectra; however, a different scaled kernel formalism was used. The absorbed scaled dose for beta kernels can be written as (*7, 31*):

$$J(r/X_{90}) = 4\pi\rho r^2 D(r)\frac{R_{CSDA}}{E_{ave}}, \tag{3}$$

where, ρ is the density of the media, r is the radial distance from the center of the sphere, $D(r)$ is the absorbed dose per source particle at radius r, X_{90} is the radius of the homogeneous sphere in which 90% of the emitted energy is absorbed, and E_{ave} is the average energy of the beta spectrum. The beta radionuclide's dose point kernels are usually scaled by using the X_{90} parameter. In this work, these parameters were

TABLE 2
CSDA Range of Electrons in Different Tissues Used for Dose Point Kernel Scaling

	R_{CSDA} range (g/cm^2)					
e$^-$ energy (MeV)	Water	Adipose	Blood	Red Marrow	Bone	Lung
0.015	5.147×10^{-4}	4.940×10^{-4}	5.198×10^{-4}	5.095×10^{-4}	5.627×10^{-4}	5.189×10^{-4}
0.05	4.320×10^{-3}	4.175×10^{-3}	4.362×10^{-3}	4.290×10^{-3}	4.681×10^{-3}	4.355×10^{-3}
0.10	1.431×10^{-2}	1.387×10^{-2}	1.445×10^{-2}	1.423×10^{-2}	1.545×10^{-2}	1.443×10^{-2}
0.50	1.766×10^{-1}	1.720×10^{-1}	1.781×10^{-1}	1.761×10^{-1}	1.898×10^{-1}	1.780×10^{-1}
1.00	4.367×10^{-1}	4.275×10^{-1}	4.413×10^{-1}	4.369×10^{-1}	4.711×10^{-1}	4.388×10^{-1}
2.00	9.875×10^{-1}	9.621×10^{-1}	9.895×10^{-1}	9.820×10^{-1}	1.056	9.719×10^{-1}
4.00	2.037	2.010	2.061	2.049	2.191	2.000
10.0	4.975	4.933	5.031	5.014	5.293	4.842

TABLE 3
The electronStepLimiter Parameters for Monoenergetic Electrons in Simulation

	electronStepLimiter (voxel size) (mm)					
e^- energy (MeV)	Water	Adipose	Blood	Red marrow	Bone	Lung
0.015	1.065×10^{-4}	1.158×10^{-4}	9.999×10^{-5}	1.034×10^{-4}	5.323×10^{-5}	4.096×10^{-4}
0.05	6.227×10^{-4}	6.768×10^{-4}	5.875×10^{-4}	6.045×10^{-4}	3.374×10^{-4}	2.395×10^{-3}
0.10	2.730×10^{-3}	2.730×10^{-3}	2.730×10^{-3}	2.650×10^{-3}	2.730×10^{-3}	1.050×10^{-2}
0.50	1.909×10^{-2}	2.074×10^{-2}	1.799×10^{-2}	1.854×10^{-2}	1.034×10^{-2}	7.342×10^{-2}
1.00	4.734×10^{-2}	4.446×10^{-2}	4.791×10^{-2}	4.601×10^{-2}	2.532×10^{-2}	1.816×10^{-1}
2.00	1.058×10^{-1}	1.150×10^{-1}	9.981×10^{-2}	1.027×10^{-1}	5.719×10^{-1}	4.070×10^{-1}
4.00	4.032×10^{-1}	4.732×10^{-1}	3.803×10^{-1}	3.913×10^{-1}	2.714×10^{-1}	1.500
10.0	5.400×10^{-1}	5.870×10^{-1}	5.099×10^{-1}	5.243×10^{-1}	2.919×10^{-1}	2.070

calculated from the simulations themselves. The numerical value of X_{90} for each simulating material-energy combination can also be calculated using,

$$4\pi\rho \int_0^{X_{90}} r^2 \Phi(r) dr = 0.90, \quad (4)$$

where $\Phi(r)$ is the fraction of energy deposited per unit mass at a distance r from a point source.

Beta spectra were simulated using the histogram option in GATE, and energy spectra of radionuclides tabulated in Table 4 were obtained from the RAdiation Dose Assessment Resource (RADAR, accessed May 2019) (*33*). It should be noted that the beta energy spectra were directly sampled during simulations instead of approximating the spectrum using a weighted sum of monoenergetic results. The average energy and the end point energy of the betas were obtained from NNDC (accessed June 2019) (*34*). In this simulation, only beta spectra are used for source input for the simulations for all isotopes.

RESULTS

Monoenergetic Electron Dose Point Kernels

The results of the simulations of dose point kernels for monoenergetic electrons are shown in Fig. 1. The DPKs have slightly different peaks in different tissues. This is because the DPKs are associated with the effective atomic number (Z_{eff}) of the media. The media that has a greater value of Z_{eff} has the highest peak (bone) in Fig. 1, and *vice versa*. This is in accordance with the stopping power theory, i.e., the proportionality of the stopping power with the ratio of atomic number and the mass number (Z/A) of the material media. The complete set of scaled dose point kernels obtained in this work for electron energies 15, 50, 100 and 500 keV, and 1, 2, 4 and 10 MeV, in water, bone, blood, red marrow, adipose and lung, are available in Supplementary Table S1 (https://doi.org/10.1667/RR15563.1.S1).

Literature Comparison of Electron Dose Point Kernels

The simulated monoenergetic electron dose point kernels were compared with those in the literature, as shown in Fig. 2. The dose point kernels generated with different Monte Carlo codes were generally in good agreement. Figure 2A shows the dose point kernels for 50 keV monoenergetic electrons in water compared to other published codes. The greatest differences occur near the maxima of the energy deposition. The maxima of dose kernels for 50 keV monoenergetic electrons generated with GATE version 8.1 is at $r/R_{CSDA} = 0.650$, i.e., 65% of the R_{CSDA} range. Other codes such as Geant4DNA and MCNPX (*9*) also appear to have maxima at $r/R_{CSDA} = 0.650$. However, for remaining codes PENELOPE (*9*) and ACCEPT (*31*), kernels show a peak at $r/R_{CSDA} = 0.600$. The largest point-to-point percentage difference between GATE version 8.1 and other codes at $r/R_{CSDA} = 0.650$ is 1.5% (PENELOPE), 3.5% (ACCEPT), 2.1% (EGSnrc), 3.8% (Geant4DNA) and 21.3% (MCNPX), respectively. However, the mean point-to-point percentage differences are 1.5% (PENELOPE), 3.1%(ACCEPT), 1.7%(EGSnrc), 2.4%(Geant4DNA) and 6.9%(MCNPX), as shown in the Fig. 3A.

For the 100 keV monoenergetic electrons, as shown in Fig. 2A, similar shapes of kernel distributions have been observed. The most significant differences were obtained at the maxima of the kernel distribution, where they amount to

TABLE 4
The electronStepLimiter Parameters for the Beta Radionuclides in Simulation

	electronStepLimiter (voxel size) (mm)					
Radionuclide	Water	Adipose	Blood	Red marrow	Bone	Lung
^{90}Y	1.106×10^{-1}	1.202×10^{-1}	1.045×10^{-1}	1.074×10^{-1}	5.979×10^{-2}	4.250×10^{-1}
^{188}Re	9.550×10^{-2}	1.040×10^{-2}	9.009×10^{-2}	9.300×10^{-2}	5.160×10^{-2}	3.670×10^{-1}
^{32}P	7.672×10^{-2}	8.320×10^{-2}	7.220×10^{-2}	7.444×10^{-2}	4.137×10^{-2}	2.949×10^{-1}
^{89}Sr	6.400×10^{-2}	6.956×10^{-2}	6.037×10^{-2}	6.210×10^{-2}	3.456×10^{-2}	2.460×10^{-1}
^{186}Re	3.860×10^{-2}	4.208×10^{-2}	3.640×10^{-2}	3.750×10^{-2}	1.937×10^{-2}	1.150×10^{-1}
^{153}Sm	2.300×10^{-2}	2.500×10^{-2}	2.050×10^{-2}	2.223×10^{-2}	1.150×10^{-2}	6.440×10^{-2}
^{177}Lu	1.210×10^{-2}	1.354×10^{-2}	1.147×10^{-2}	1.175×10^{-2}	6.500×10^{-2}	4.549×10^{-2}

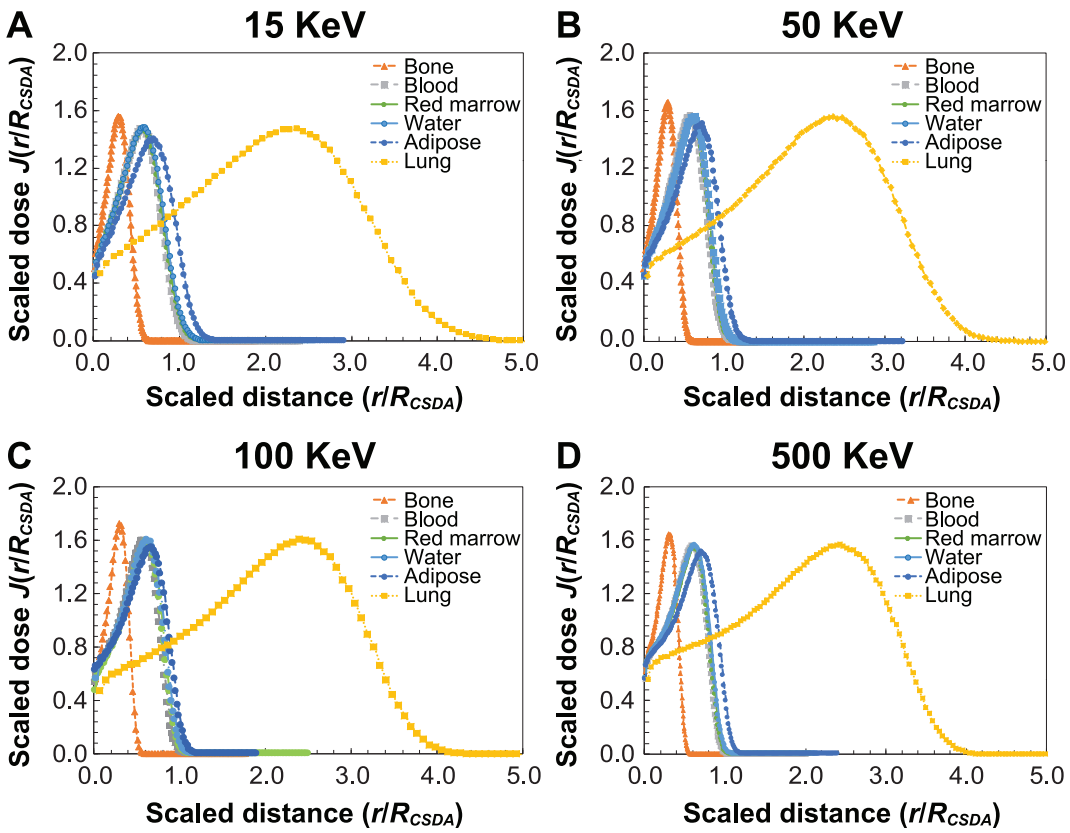

FIG. 1. Panels A–D: Dose point kernels of 15, 50, 100 and 500 keV monoenergetic electrons, respectively, in water, bone, blood, adipose, red marrow and lung.

less than 6% for the PENELOPE, ACCEPT, EGSnrc and Geant4DNA codes, and ~2% for MCNPX code, respectively. However, the mean percentage differences are slightly less than that of 50 keV monoenergetic electrons (Fig. 3). For the 1 MeV electrons in water, similar discrepancies were observed and are comparable to the variations between other Monte Carlo codes. Overall, there is a good agreement between the codes.

Dose point kernels in bone are not available in the literature for all electron energies simulated herein, so comparisons were only made for 1 MeV monoenergetic electrons. Comparison between the results of our study with FLUKA (*8*) and GATE version 6.1 (*11*) are favorable, with 3.4% and 1.1% differences.

Tissue-Specific Beta-Emitting Radionuclide Dose Point Kernels

The numerical values of X_{90} were calculated based on the 90% total energy deposited by all the primary events. The corresponding radius of the concentric spheres at 90% total energy deposited value gives the X_{90} metric. The X_{90} values simulated herein are included in Table 5. The simulated values in water agree with values reported in the literature. The large differences in X_{90} values in Table 5 as a function of tissue type are primarily driven by the density of tissue. The results of the simulation of beta dose point kernels for ^{90}Y, ^{32}P, ^{188}Re, ^{186}Re, ^{89}Sr, ^{153}Sm and ^{177}Lu isotopes in water, bone, blood, red marrow, adipose and lung are shown in the Figs 4, 5 and 6. The complete data are available in Supplementary Table S2 (https://doi.org/10.1667/RR15563.1.S1).

As shown in Figs. 4 and 5, the beta dose point kernels in different media do not differ significantly when normalized to X_{90}. To quantify the differences between kernels, the mean percentage difference between the point-to-point comparison of dose point kernels for ^{177}Lu has been calculated using Eq. (5) for all tissue types. The point-to-point comparison of the two-dose point kernel profiles at the same scaled distance from the source can be calculated using Eq. (5),

$$\%\ \text{mean difference} = \frac{1}{N}\left[\frac{\sum_{i=1}^{N}(J_{w,i}(r/X_{90}) - J_{t,i}(r/X_{90}))}{max(J_{w,i}(r/X_{90}), J_{t,i}(r/X_{90}))}\right] \times 100\%, \quad (5)$$

where, $J_w(r/X_{90})$ is the dose point kernel in water at the scaled distance (r/X_{90}) and $J_t(r/X_{90})$ is the dose point kernel at the same scaled distance (r/X_{90}) in other tissues; namely bone, blood, adipose, lung and red marrow, and N represents the total number of points in calculation.

The average statistical uncertainties in all beta simulations are less than 5% for $0.1 < (r/X_{90}) < 1.0$. The beta DPKs of

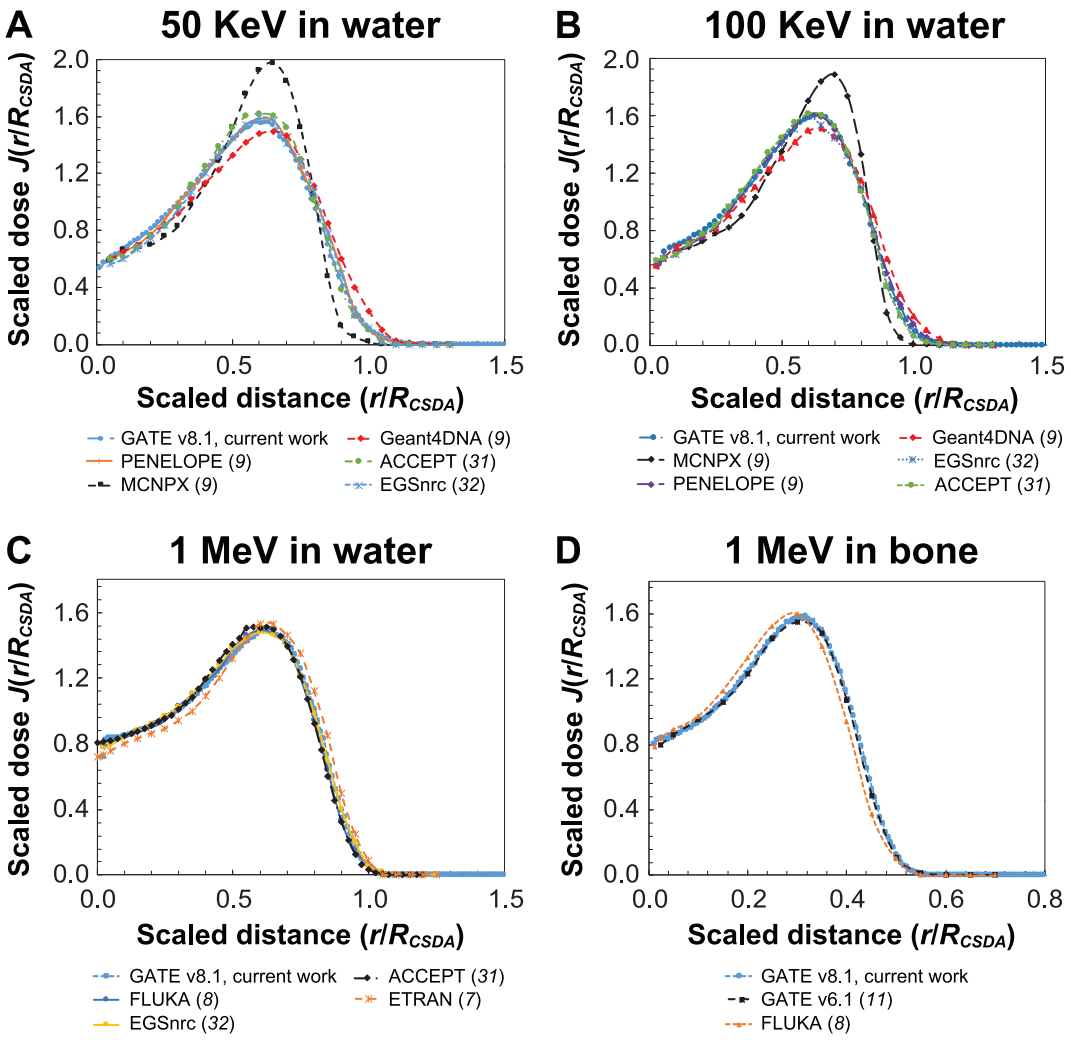

FIG. 2. Comparison of DPKs of monoenergetic electrons with published kernels of (panels A–C) 50 keV, 100 keV and 1 MeV, respectively, in water and (panel D) 1 MeV in bone.

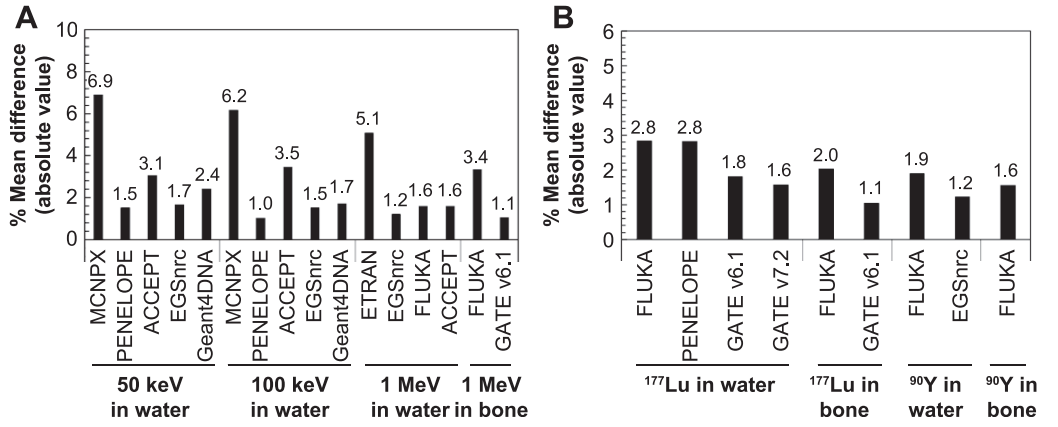

FIG. 3. Mean percentage deviation from other published works (8, 11, 32) for (panel A) monoenergetic electrons in water (50 keV, 100 keV, 1 MeV) and 1 MeV monoenergetic electrons in bone and (panel B) ^{177}Lu and ^{90}Y beta dose point kernels in water and bone.

TABLE 5
X_{90} Values Calculated from Simulated Dose Point Kernels

Radionuclide	X_{90} values (mm)						X_{90} values in water (mm) in the literature
	Bone	Blood	Red marrow	Water	Adipose	Lung	
^{90}Y	2.93	5.09	5.33	5.39	5.85	20.36	5.40 (*8*), 5.43 (*32*)
^{188}Re	2.60	4.43	4.65	4.71	5.15	18.05	4.57 (*8*), 4.89 (*35*)
^{32}P	2.13	3.68	3.81	3.86	4.25	14.95	3.66 (*32*), 3.74 (*36*)
^{89}Sr	1.81	3.21	3.24	3.28	3.62	12.36	3.21 (*36*)
^{186}Re	1.24	2.14	2.23	2.25	2.47	8.71	1.91 (*8*)
^{153}Sm	0.65	1.15	1.19	1.20	1.32	4.65	1.15 (*8*)
^{177}Lu	0.36	0.63	0.65	0.66	0.73	2.57	0.62 (*8*)

^{177}Lu and ^{90}Y in different media are shown in Figs. 4 and 5. The mean percentage difference between the beta DPKs in water to those in bone, blood, lung, adipose and red marrow are less than 2% (Fig. 4A). The calculated discrepancies are not statistically significant.

Figure 6 shows the beta radionuclide dose point kernels plotted with the scaled distance and the radial distance in water, bone, blood and lung. All the DPKs plotted with the scaled distance (Fig. 6A, C, E and G) and the radial distances (Fig. 6B, D, F and G) in different tissues are found to be similar in shape and magnitude.

Literature Comparison of Beta Dose Point Kernels

Although beta kernels were generated for water, bone, blood, red marrow, adipose and lung, comparison against the data found in the literature is only possible for water and bone. These comparisons are shown in Figs. 7 and 8. This work using GATE versions 8.1 and 7.2 shows an excellent agreement with the dose point kernels calculated using FLUKA and PENELOPE Monte Carlo codes.

Discrepancies among kernels were quantified for scaled distances (r/X_{90}) < 1. The beta dose point kernels of ^{177}Lu were compared to those of FLUKA (*8*), PENELOPE (*8*) and earlier versions of GATE [version 6.1 (*11*) and version 7.2 (current work)] in water and bone media. Similarly, the beta kernels of ^{90}Y were compared using FLUKA (*8*) and EGS4 (*32*) in water and bone. The small deviations between dose kernels in Figs. 7 and 8 are likely caused by different values for the X_{90} parameter in addition to differences between Monte Carlo codes. The mean percentage difference in dose kernels obtained in the current work compared to that of the literature has been calculated and shown in Fig. 3A. The results show the excellent agreement between the codes, and the mean differences between the GATE and other codes range between 1% and 3%.

DISCUSSION

There has been significant interest in developing new 3D dosimetry tools for targeted radionuclide therapy. This interest is motivated by the shortcomings of utilizing pre-tabulated energy transfer coefficients generated from virtual anthropomorphic phantoms. So-called ‘‘voxel-wise dosimetry’’ aims to provide a dose or dose-rate estimate for each voxel within a nuclear medicine image volume. The most straightforward approach using dose point kernel voxel-wise dosimetry involves convolving an isotope-specific energy deposition kernel with the activity map. However, this approach neglects the impact of tissue type and density heterogeneity within the patient. The use of tissue-specific VSV or DPK in different tissue interfaces, e.g., at soft tissue/bone, lung/soft tissue interfaces or lung/bone, is still a challenge. More research is needed to study the behavior of kernels at such interfaces. The goal of this work was to: 1. Improve the availability of electron and beta kernels in

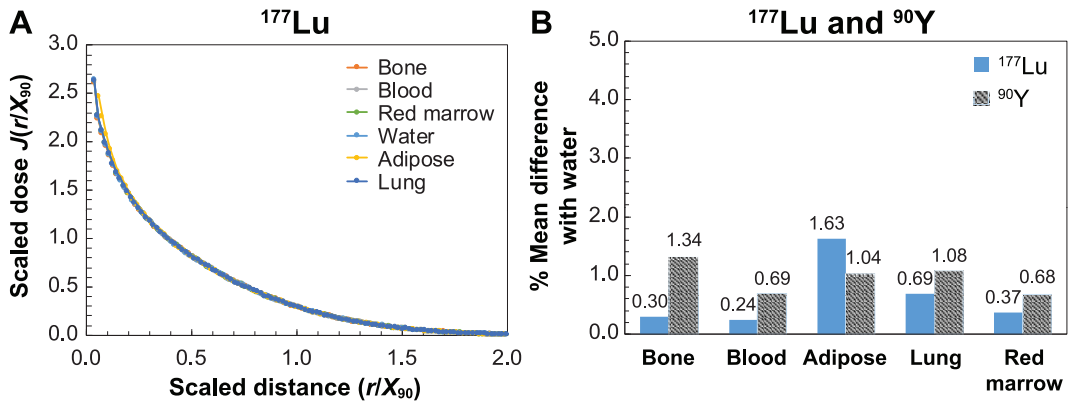

FIG. 4. Panel A: Beta DPKs for ^{177}Lu in bone, blood, red marrow, water, adipose and lung. Panel B: Beta DPKs of ^{177}Lu and ^{90}Y in water compared with other tissues.

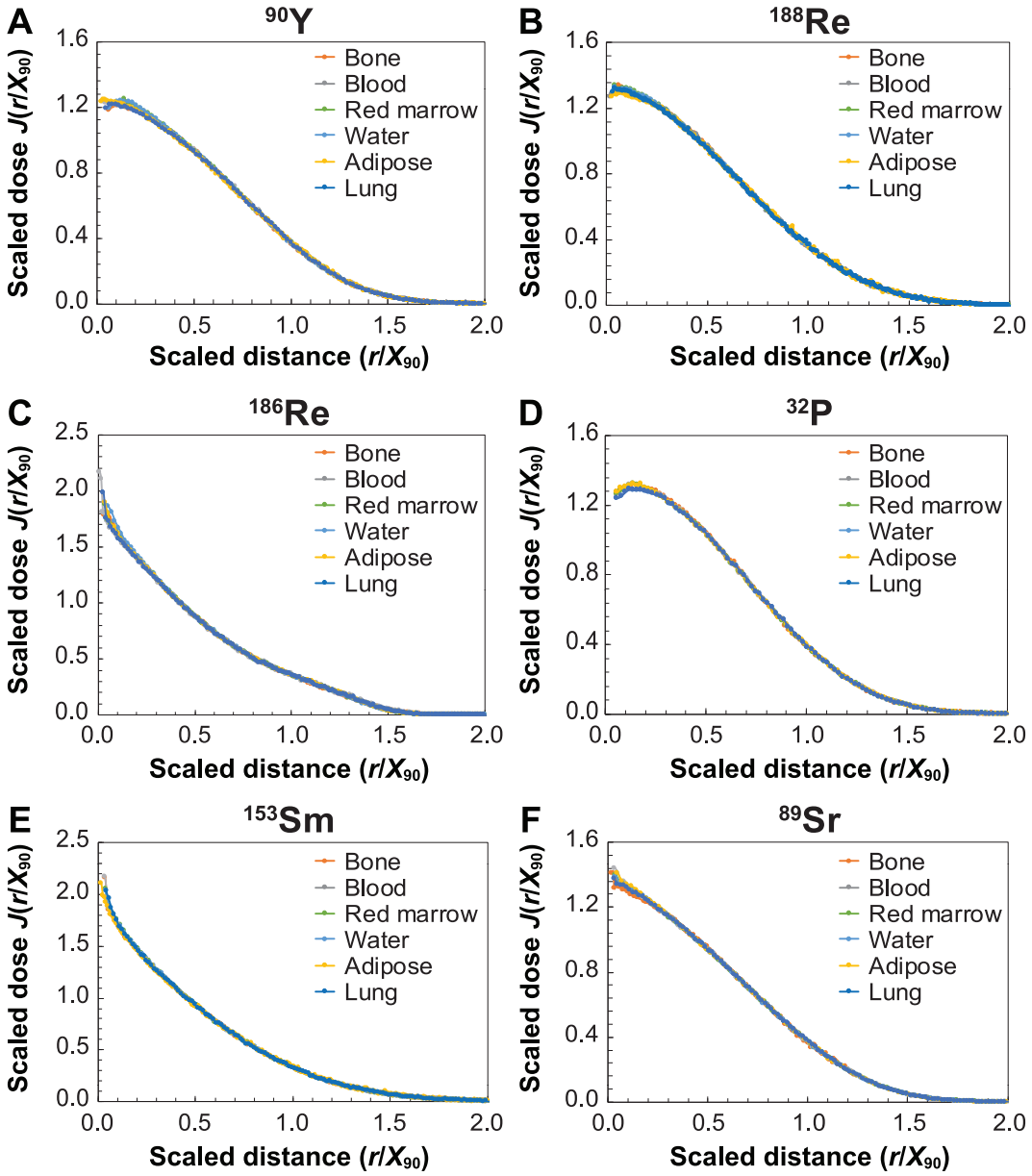

FIG. 5. Panels A–F: Dose point kernels of the beta emitters ^{90}Y, ^{188}Re, ^{186}Re, ^{32}P, ^{153}Sm and ^{89}Sr nuclides, respectively, in water, bone, blood, red marrow, adipose and lung as a function of scaled distance (r/X_{90}).

literature; and 2. To assess the importance of utilizing tissue-specific electron kernels for voxel-wise dosimetry.

GATE is a validated Monte Carlo simulation toolkit for tomographic emission, radiotherapy and dosimetric applications. In recent years, GATE has been widely implemented for different studies on the radiation transport field (*11, 20, 21, 23*). It has been gaining popularity because of its versatility, its scripting mechanism, powerful visualization and 3D rendering tools. Ferrer *et al.* (*20*) were the first to use GATE for monoenergetic electron dose point kernel simulations in water using Geant4 4.8.1. In addition, Maigne *et al.* (*21*) simulated monoenergetic electrons in water using GATE version 6.0. Furthermore, Papadimitroulas *et al.* (*11*) implemented GATE version 6.1 to simulate the beta radionuclides and monoenergetic electrons in water, bone, lung and soft tissue. Since the currently available voxel-wise approaches to radionuclide dosimetry ignore tissue composition and do not account for density heterogeneities, a study on the impact of tissue type on dose point kernels was deemed necessary. Thus, we studied the impact of tissue types on dose point kernels for radionuclides that are widely used in nuclear medicine.

In this work, dose point kernels have been simulated with GATE Monte Carlo code for both monoenergetic electrons and beta radionuclides in water, compact bone, blood, red marrow, adipose and lung. The resulting dose point kernels are in excellent agreement with published data. The maximum discrepancy observed in this work is 7%

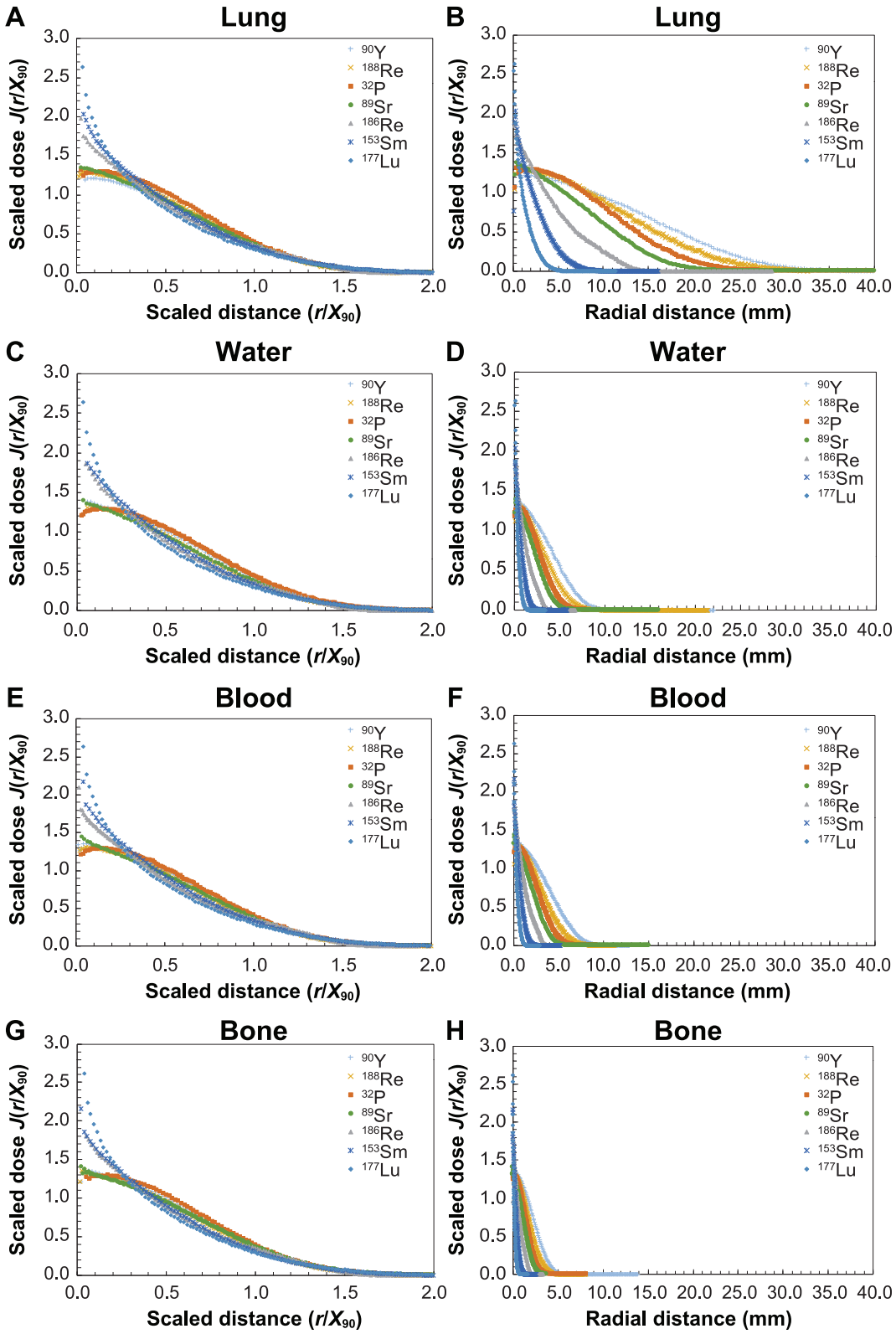

FIG. 6. DPKs of beta radionuclides plotted with scaled distance and radial distance in (panels A and B) lung, (panels C and D) water, (panels E and F) blood and (panels G and H) bone. The abscissa and ordinates are scaled similarly for ease of comparison.

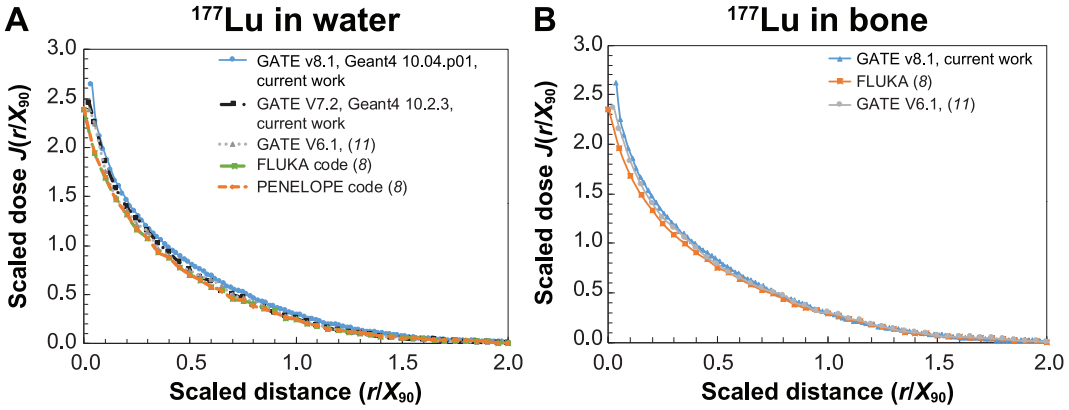

FIG. 7. Comparison against literature kernels for ^{177}Lu in (panel A) water and (panel B) bone.

compared to MCNPX and ETRAN code. The observed discrepancies in the dose point kernels may be due to the superposition of multiple factors. The significant contributions are likely from the following: 1. X_{90} values used in scaling of kernels; 2. Differences in the average energy of the radionuclides in literature; 3. Beta spectra used in the radionuclide simulation; and 4. Different treatment of charged particle transport among Monte Carlo codes.

The X_{90} value reported by Mainegra-Hing *et al.* (*32*) for ^{90}Y does not greatly differ from the value calculated in the current work. However, Botta *et al.* (*8*) reported a slightly higher value as shown in Table 5. In addition, for ^{188}Re, Mainegra-Hing *et al.* (*32*) reported a smaller value, whereas Botta *et al.* (*8*) reported a higher value than the calculated value. Similar discrepancies were observed for all other radionuclide dose kernel simulations.

Differences among Monte Carlo codes are expected, due to differences in their treatment of electron transport. The Monte Carlo codes MCNPX and ETRAN utilize the condensed history algorithm, and PENELOPE makes use of a mixed simulation algorithm that combines both the detailed and condensed history algorithm. In addition, EGSnrc exploited the Molière multiple scattering model with an exact boundary crossing algorithm and FLUKA code based on the multiple scattering model. However, GATE used in this work incorporates Geant4 source code and employs the revised electron multiple scattering algorithm along with the physics list mechanism; in GATE, a physics list is a mandatory user input.

For the beta radionuclide simulations, all beta energy spectra were obtained from the RADAR website (*33*). Only beta spectra were included in radioisotope simulations, which excludes internal conversion electrons, Auger electrons, X and gamma rays contribution of the radionuclide decay process. Simulation of beta spectra is sufficient to understand the impact of tissue type on dose point kernels. However, if one wants to use these kernels in clinical dosimetry, they should be supplemented with the missing decay modes.

Results of the beta dose kernel simulations show a discrepancy of 3.0%, compared to results found in the literature, FLUKA code (*8*). This is likely due to inclusion of Auger electrons, conversion electrons and photons within the FLUKA simulations. In addition, deviation from results obtained by Papadimitroulas *et al.* (*11*) is likely due to the fact that they derived the beta spectra from the LBNL database in their study and implemented an earlier version of GATE. The observed discrepancy in this study, compared to GATE version 6.1 (*11*), is less than 2.0%.

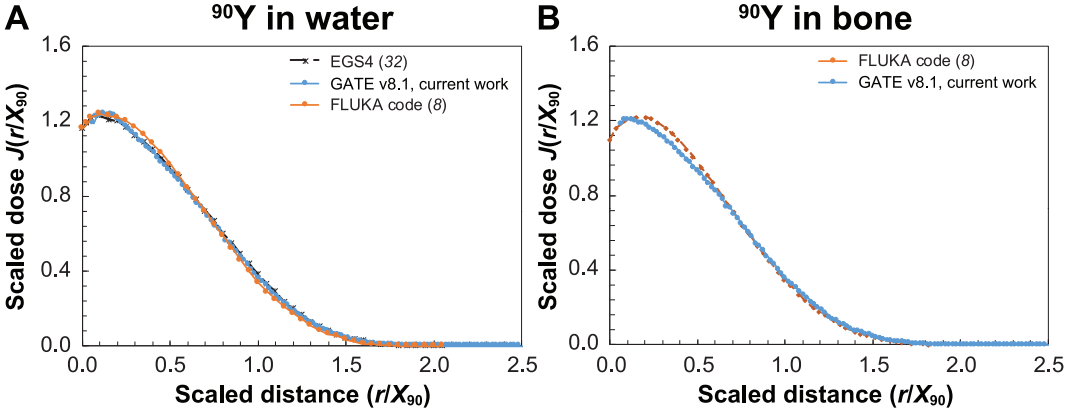

FIG. 8. Comparison against literature kernels for ^{90}Y in (panel A) water and (panel B) bone.

In this work, we did not include X-ray generation during charged particle transport. Therefore, the resulting dose point kernels include only the collisional electron stopping power. Based on the elemental composition of tissues, GATE calculates the mean excitation energies. The calculated mean excitation energies for the adipose, red marrow, water, lung, blood and bone are, respectively, 61.75, 66.21, 68.99, 69.73, 69.80 and 86.00 eV. Note that these calculated values differ slightly from values reported in the NIST online database (*30*). According to the Bethe-Bloch theory of electron stopping power, the collisional mass stopping power varies linearly with the ratio of atomic number and the mass number (Z/A). The Z_{eff} values of the simulated tissues are 11.87 (bone), 7.78 (blood), 7.74 (lung), 7.42 (water), 7.21 (red marrow) and 6.47 (adipose), respectively. As the Z_{eff} and the mean excitation energy (I) values do not greatly differ from each other except for bone, stopping power will have similar values for the same radionuclide. However, for bone, a slightly larger value of the mean excitation energy serves to counteract the increase in average atomic number yielding dose point kernels that are comparable to water.

Mean percentage deviation of tissue-specific kernels compared with water was less than 2% for all comparisons. This result is supported by stopping power theory and suggests that tissue composition heterogeneity is a second-order effect with regard to energy deposition. As expected, tissue density appears to be a more critical variable that dramatically impacts DPK shapes. This suggests that water kernels alone can adequately describe energy deposition in tissue from electron-emitting sources as long as we carefully account for the densities of tissues such as lung, bone and adipose when calculating the dose distributions.

CONCLUSION

We report the generation of dose point kernels for medically-relevant radioisotopes in water, compact bone, lung, adipose, blood and red marrow. The impact of tissue types on dose point kernels has been studied using the GATE version 8.1 Monte Carlo toolkit. Also discussed here were the major contributing factors that result in uncertainties in dose point kernel simulations. Previously unreported kernels that have been generated herein include those for ^{90}Y, ^{188}Re, ^{32}P, ^{89}Sr, ^{186}Re, ^{153}Sm and ^{177}Lu radionuclides, and 0.015–10 MeV monoenergetic electrons, in blood, red marrow, lung and adipose. Tissue type had minimal impact for purposes of dosimetry, suggesting that the use of a single kernel generated in water may be suitable for voxel-wise calculations, providing that tissue-specific density corrections are implemented.

SUPPLEMENTARY INFORMATION

Supplementary Tables S1 and S2 comprise all simulated monoenergetic electrons and radionuclide beta spectrum dose point kernel data, respectively, in different tissue types. The notations used in the Supplementary Tables are in agreement with those used in this article.

ACKNOWLEDGMENTS

This research was supported in part through computational resources provided by The University of Iowa, Iowa City, Iowa. The authors would like to thank Glenn Johnson for his help in configuring GATE for use on the university Argon cluster.

Received: November 11, 2019; accepted: March 11, 2020; published online: April 21, 2020

REFERENCES

1. Prise KM, O'Sullivan JM. Radiation-induced bystander signalling in cancer therapy. Nat Rev Cancer 2009; 9:351–60.
2. Bolch WE, Eckerman KF, Sgouros G, Thomas SR. MIRD Pamphlet No. 21: A Generalized schema for radiopharmaceutical dosimetry-standardization of nomenclature. J Nucl Med 2009; 50:477–84.
3. Bolch WE, Bouchet LG, Robertson JS, Wessels BW, Siegel JA, Howell RW, et al. MIRD pamphlet No. 17: The dosimetry of nonuniform activity distributions - Radionuclide S values at the voxel level. J Nucl Med 1999; 40:11s–36s.
4. Dieudonne A, Hobbs RF, Bolch WE, Sgouros G, Gardin I. Fine-resolution voxel S values for constructing absorbed dose distributions at variable voxel size. J Nucl Med 2010; 51:1600–7.
5. Grimes J, Celler A. Comparison of internal dose estimates obtained using organ-level, voxel S value, and Monte Carlo techniques. Med Phys 2014; 41.
6. Huizing DMV, de Wit-van der Veen BJ, Verheij M, Stokkel MPM. Dosimetry methods and clinical applications in peptide receptor radionuclide therapy for neuroendocrine tumours: A literature review. EJNMMI Res 2018; 8:89.
7. Berger MJ. Improved point kernels for electron and beta-ray dosimetry. NBSIR Report No. 73-107. Washington, DC: U.S. Atomic Energy Commission 1973.
8. Botta F, Mairani A, Battistoni G, Cremonesi M, Di Dia A, Fasso A, et al. Calculation of electron and isotopes dose point kernels with FLUKA Monte Carlo code for dosimetry in nuclear medicine therapy. Med Phys 2011; 38:3944–54.
9. Champion C, Incerti S, Perrot Y, Delorme R, Bordage MC, Bardies M, et al. Dose point kernels in liquid water: An intra-comparison between GEANT4-DNA and a variety of Monte Carlo codes. Appl Radiat Isot 2014; 83:137–41.
10. Furhang EE, Sgouros G, Chui CS. Radionuclide photon dose kernels for internal emitter dosimetry. Med Phys 1996; 23:759–64.
11. Papadimitroulas P, Loudos G, Nikiforidis GC, Kagadis GC. A dose point kernel database using GATE Monte Carlo simulation toolkit for nuclear medicine applications: comparison with other Monte Carlo codes. Med Phys 2012; 39:5238–47.
12. Prestwich WV, Nunes J, Kwok CS. Beta dose point kernels for radionucides. J Nucl Med 1989; 30:1036–46.
13. Simpkin DJ, Mackie TR. Egs4 Monte-Carlo determination of the beta-dose kernel in water. Med Phys 1990; 17:179–86.
14. Uusijarvi H, Chouin N, Bernhardt P, Ferrer L, Bardies M, Forssell-Aronsson E. Comparison of electron dose-point kernels in water generated by the Monte Carlo codes, PENELOPE, GEANT4, MCNPX, and ETRAN. Cancer Biother Radiopharm 2009; 24:461–7.
15. Seltzer SM. Electron photon Monte-Carlo calculations - the Etran code. Appl Radiat Isot 1991; 42:917–41.
16. Graves SA, Flynn RT, Hyer DE. Dose point kernels for 2,174 radionuclides. Med Phys 2019; 46:5284–93.

17. OpenGATE Collaboration, GATE users guide version 8.0. 2004. (http://bit.ly/2YYEKOK)

18. Jan S, Santin G, Strul D, Staelens S, Assie K, Autret D, et al. GATE: A simulation toolkit for PET and SPECT. Phys Med Biol 2004; 49:4543–61.

19. Visvikis D, Bardies M, Chiavassa S, Danford C, Kirov A, Lamare F, et al. Use of the GATE Monte Carlo package for dosimetry applications. Nucl Instrum Methods Phys Res A 2006; 569:335–40.

20. Ferrer L, Chouin N, Bitar A, Lisbona A, Bardies M. Implementing dosimetry in GATE: Dose-point kernel validation with GEANT4 4.8.1. Cancer Biother Radiopharm 2007; 22:125–9.

21. Maigne L, Perrot Y, Schaart DR, Donnarieix D, Breton V. Comparison of GATE/GEANT4 with EGSnrc and MCNP for electron dose calculations at energies between 15 keV and 20 MeV. Phys Med Biol 2011; 56:811–27.

22. Marcatili S, Villoing D, Mauxion T, McParland BJ, Bardies M. Model-based versus specific dosimetry in diagnostic context: Comparison of three dosimetric approaches. Med Phys 2015; 42:1288–96.

23. Sarrut D, Bardies M, Boussion N, Freud N, Jan S, Letang JM, et al. A review of the use and potential of the GATE Monte Carlo simulation code for radiation therapy and dosimetry applications. Med Phys 2014; 41.

24. Thiam CO, Breton V, Donnarieix D, Habib B, Maigne L. Validation of a dose deposited by low-energy photons using GATE/GEANT4. Phys Med Biol 2008; 53:3039–55.

25. Kawashima H. Radioimmunotherapy: a specific treatment protocol for cancer by cytotoxic radioisotopes conjugated to antibodies. ScientificWorldJournal 2014; 2014:492061.

26. Allison J, Amako K, Apostolakis J, Arce P, Asai M, Aso T, et al. Recent developments in GEANT4. Nucl Instrum Methods Phys Res A 2016; 835:186–225.

27. Photon, electron, proton and neutron interaction data for body tissues. ICRU Report No. 46. Bethesda, MD: International Commission on Radiation Units and Measurements; 1992.

28. Briesmeister JF. MCNP-A general Monte Carlo N-particle transport code. Report No. LA-13181. Los Alamos, NM: Los Alamos National Laboratory; 1997.

29. Agostinelli S, Allison J, Amako K, Apostolakis J, Araujo H, Arce P, et al. GEANT4-a simulation toolkit. Nucl Instrum Methods Phys Res A 2003; 506:250–303.

30. Berger MJ, Coursey JS, Zucker MA. ESTAR, PSTAR, and ASTAR: computer programs for calculating stopping-power and range tables for electrons, protons, and helium ions (version 1.21). Gaithersburg, MD: National Institute of Standards and Technology (NIST); 1999

31. Cross WG, Freedman NO, Wong PY. Beta-ray dose distributions from point sources in an infinite water medium. Health Phys 1992; 63:160–71.

32. Mainegra-Hing E, Rogers DWO, Kawrakow I. Calculation of photon energy deposition kernels and electron dose point kernels in water. Med Phys 2005; 32:685–99.

33. Stabin MG, Siegel JA, Hunt J, Sparks R, Lipsztein J, Eckerman KF. RADAR: the radiation dose assessment resource–an online source of dose information for nuclear medicine and occupational radiation safety [abstract]. J Nucl Med 2002; 42:243p.

34. NuDat (Nuclear Structure and Decay Data). Upton, NY: National Nuclear Data Center, Brookhaven National Laboratory; 2008.

35. Hamby DM, Mangini CD, Caffrey JA, Tang M. VARSKIN 5: A computer code for skin contamination dosimetry. Corvallis, OR: Department of Nuclear Engineering and Radiation Health Physics, Oregon State University; 2014.

36. Mayles P, Nahum A, Rosenwald JC, Papanikolaou N. Handbook of radiotherapy physics: Theory and practice. 1st ed. Boca Raton, FL: J.C. Taylor & Francis Group, CRC Press; 2008.